Preprints.org

Article

Not peer-reviewed version

Mitochondrial Graph-Based Pan-Genome Analysis of *Hypsizygus Marmoreus*: Structural Variation, Adaptive Evolution and Its Implications for Germplasm Resource Improvement

Ruichen Ma , Wenyun Li , Yongmei Miao , Ruiheng Yang , Youran Shao , Junjun Shang , Yan Li , Yuan Gao , Dapeng Bao * , Yingying Wu *

Posted Date: 28 February 2026

doi: 10.20944/preprints202602.1502.v1

Keywords: *Hypsizygus marmoreus*; mitochondria; structural variation; graph-based pan-genome; fungal genetics

Preprints.org is a free multidisciplinary platform providing preprint service that is dedicated to making early versions of research outputs permanently available and citable. Preprints posted at Preprints.org appear in Web of Science, Crossref, Google Scholar, Scilit, Europe PMC.

Copyright: This open access article is published under a Creative Commons CC BY 4.0 license, which permit the free download, distribution, and reuse, provided that the author and preprint are cited in any reuse.

Preprints.org (www.preprints.org) | NOT PEER-REVIEWED | Posted: 28 February 2026 doi:10.20944/preprints202602.1502.v1

Disclaimer/Publisher's Note: The statements, opinions, and data contained in all publications are solely those of the individual author(s) and contributor(s) and not of MDPI and/or the editor(s). MDPI and/or the editor(s) disclaim responsibility for any injury to people or property resulting from any ideas, methods, instructions, or products referred to in the content.

Article

Mitochondrial Graph-Based Pan-Genome Analysis of *Hypsizygus Marmoreus*: Structural Variation, Adaptive Evolution and Its Implications for Germplasm Resource Improvement

Ruichen Ma [1,†], Wenyun Li [2,†], Yongmei Miao [1], Ruiheng Yang [2,3], Youran Shao [2], Junjun Shang [2,3], Yan Li [2,3], Yuan Gao [2], Dapeng Bao [2,3,*] and Yingying Wu [2,3,*]

[1] Anhui Science and Technology University, Fengyang 233100, China

[2] National Engineering Research Center of Edible Fungi, Key Laboratory of Applied Mycological Resources and Utilization, Ministry of Agriculture, Institute of Edible Fungi, Shanghai Academy of Agricultural Sciences, Shanghai 201403, China

[3] Shanghai Key Laboratory of Agricultural Genetics and Breeding, Shanghai Academy of Agricultural Sciences, Shanghai 201106, China

* Correspondence: baodapeng@saas.sh.cn(D.B.); wuyingying@sibs.ac.cn(Y.W.)

† These authors contributed equally to this work and share first authorship.

Abstract

As semi-autonomous organelles, mitochondria function through the coordinated regulation of nuclear genomes and their own genetic material, primarily providing energy for eukaryotic organisms. Currently, high-throughput sequencing technologies have been used to resolve the mitochondrial genomes of various edible fungi. With advances in sequencing technology, species genome characterization has evolved from single genomes to pan-genomes. However, the application of pan-genomes for the analysis of edible mushroom mitochondrial genomes remains unexplored. In this study, we conducted a comparative mitochondrial genome analysis of 31 *Hypsizygus marmoreus* strains (4 newly sequenced monotypes and 27 public datasets). The results revealed that the mitochondrial genome sizes ranged from 98,284 to 111,087 bp, exhibiting significant structural diversity. This variation is primarily driven by dynamic changes in non-coding regions, particularly intronic polymorphisms in the *cox1* gene. This study revealed that tRNA secondary structures exhibit atypical globular and elongated conformations alongside copy number variations. Additionally, codon usage showed a pronounced A/T bias, whereas core respiratory chain genes demonstrated an evolutionary pattern of strong purifying selection. Furthermore, the 31 mitochondrial genomes of *H. marmoreus* were identified 8 gene rearrangement patterns and 5 genetic clusters, and the pan-genome (220,364 bp, 217 nodes) captured abundant SNPs, InDels and structural variations. This study provides breeding-relevant genetic markers and a genomic framework for germplasm classification, genetic improvement and stress-resilient variety molecular breeding of *Hypsizygus marmoreus*.

Keywords: *Hypsizygus marmoreus*; mitochondria; structural variation; graph-based pan-genome; fungal genetics

1. Introduction

Hypsizygus marmoreus, an edible macrofungus belonging to the Basidiomycota phylum, Agaricomycetes class, Agaricales order, Lyophyllaceae family, and *Hypsizygus* genus, is commercially cultivated as white and brown strains [1]. It is very popular in East and Southeast Asia. Due to its smooth, crisp and tender texture, unique aroma, and shape similar to *Tricholoma matsutake*,

© 2025 by the author(s). Distributed under a Creative Commons CC BY license.

Preprints.org (www.preprints.org) | NOT PEER-REVIEWED | Posted: 28 February 2026 doi:10.20944/preprints202602.1502.v1

it is called "false *T. matsutake*" in Japan. Previous studies of *H. marmoreus* have primarily focused on functional genes [2], nutrients, bioactive compounds [3], and mating-type genes [4]. Although multiple mitochondrial genomes of *H. marmoreus* have been sequenced and published, previous studies have mostly concentrated on the annotation of individual genomes or limited comparative analyses [5,6]. However, there is still a lack of a graph-based pan-genomic perspective to systematically elucidate the intraspecific structural variation of *H. marmoreus*, and the application of mitochondrial genomic variation in its germplasm classification and molecular breeding has not been explored. As a commercially important edible fungus, the innovation of germplasm resources and the development of molecular breeding technology are the core to improve its cultivation efficiency and stress resistance, and the mitochondrial genome, as a key cytoplasmic genetic resource, is of great significance for its molecular regulation and germplasm preservation.

The mitochondrial genome is a segment of genetic material that exists in the cytoplasm and encodes key proteins and RNA molecules involved in cellular energy metabolism [7]. In fungi, this structure appears in a ring shape, interacting with, and remaining isolated from, the nuclear genome. The main difference is that the rate of sequence variation is relatively fast and significantly higher than that in the nuclear genome, whereas it is relatively conserved in terms of protein encoding[8]. Kim et al. analyzed tandem repeat sequences and *A*-matching types of mitochondrial genes in *Lentinus edodes*, hypothesized that the differences in tandem repeats were closely related to the evolutionary process, and used these tandem repeat sequences for molecular labeling to screen for suitable high-potential strains with nuclear-cytoplasmic matching[9]. Song et al. replaced the mitochondria within *L. edodes* cells and analyzed the impact of browning during the coloring stage based on transcriptome data [10]. They found that the mitochondria were associated with the color and stem length of *L. edodes*. Wu et al. conducted a comparative analysis of intron dynamics and gene rearrangements in the mitochondrial genomes of two saprotrophic *Coniophora* species, which may aid in understanding the origin and evolutionary patterns of boletes[11]. Tan et al. conducted a comparative analysis of mitochondrial genomes from 46 strains of *Flammulina filiformis*, identified polymorphisms in the *cox1* intron and intergenic regions, and designed primers to identify mitochondrial differentiation [12]. The mitochondrial genomes of 361 *Agaricus bisporus* individuals revealed the global evolutionary process and domestication history of the species [13]. These studies show that the mitochondrial genome not only contains important genes related to the growth and development of edible fungi but also serves as a valuable resource for studying population genetics and evolutionary history.

With the decline in sequencing costs and innovation of analytical methods, Pan-genome research has expanded from nuclear genomes to organelle genomes. The Pan-mitogenome can systematically reveal the genetic diversity, adaptability, and evolutionary mechanisms of a species by integrating the mitochondrial information of multiple strains[14,15]. Graph-structured pan-genomes can efficiently store and visualize complex sequence variations (such as single nucleotide polymorphisms and indels) and SVs (such as gene rearrangements and insertions/deletions), thereby significantly enhancing the ability to analyze the dynamics of genomic structures [16]. Although this method has shown potential in the medical research of animals, plants, and humans, it is still underdeveloped in the field of edible fungi, especially in research related to mitochondrial SVs in *H. marmoreus*.

To investigate the pan-mitogenome characteristics of *H. marmoreus*, we performed whole-genome sequencing of two pairs of compatible monokaryons (f2, f4, nn12-1, and nn12-17) derived from two commercial strains with superior traits. These data were integrated with 27 publicly available *H. marmoreus* genomic datasets in the NCBI database. A comprehensive analysis of the composition of mitochondrial protein-coding genes (PCGs), tRNA secondary structures, repetitive sequences, codon usage bias, evolutionary selection pressure, and nucleotide diversity was conducted. Subsequently, we employed phylogenetic reconstruction, population structure analysis, and mitochondrial graph-based pan-genome methods to systematically explore the evolutionary patterns and genetic variation profiles of the *H. marmoreus* mitogenome. Ultimately, this study aims to construct the first graph-based mitochondrial pan-genome of *H. marmoreus*, explore its

© 2025 by the author(s). Distributed under a Creative Commons CC BY license.

Preprints.org (www.preprints.org) | NOT PEER-REVIEWED | Posted: 28 February 2026 doi:10.20944/preprints202602.1502.v1

evolutionary characteristics and structural variation rules, and provide breeding-relevant genetic markers and genomic framework for the germplasm improvement, molecular breeding and germplasm preservation of *H. marmoreus*.

2. Materials and Methods

2.1. Experimental Strains and Data Sources

The monokaryotic strains of *H. marmoreus* (f2, f4, nn12-1, and nn12-17) used in this study, whose GenBank accession numbers are PV946885, PX600725, PX600726, and PX600727 respectively, are preserved by the National Edible Fungi Germplasm Resource Bank (Shanghai), Ministry of Agriculture and Rural Affairs, P.R. China. Among them, f2 and f4 are a pair of compatible monokaryons isolated from the white commercial strain of *H. marmoreus* Finc-W-247 (CGMCC 13193), which produces pure white, translucent fruiting bodies with regular, non-cracking pilei, long shelf life and crisp, tender, smooth flesh. Similarly, nn12-1 and nn12-17 are a pair of compatible monokaryons derived from the brown commercial strain *H. marmoreus* NN-12 (introduced from Japan), characterized by marbled pilei, thick and firm texture, long shelf life, and a distinctive crab-like flavor. Additionally, two complete mitochondrial genomes and 25 whole-genome sequencing datasets of *H. marmoreus* were downloaded from the NCBI database for subsequent integrated analysis [6].

2.2. Mycelium Collection

Strains f2, f4, nn12-1, and nn12-17 were inoculated onto PDA medium (39 g potato dextrose agar powder, distilled water to 1 L, sterilized at 121 °C for 20 min before use). The cultures were incubated at 23 °C until mycelium growth reached the outer two-thirds of the 90 mm plate. Under sterile conditions, 10 g of mycelium was scraped, rapidly frozen in liquid nitrogen, and stored at -80 °C for subsequent genomic sequencing.

2.3. Genome Sequencing, Assembly, and Annotation

Genome sequencing of the four experimental strains was performed using PacBio Sequel and Illumina NovaSeq platforms. Second-generation sequencing depth ranged from 30 to 41x with coverage of 1.23-1.65 GB, while third-generation high-fidelity (HiFi) sequencing depth reached 100 to 175x with coverage of 4.0-6.9 GB. Based on this, the sequencing data of the mitochondrial genome obtained in this study has a coverage depth ranging from 2,441x to 4,616x, corresponding to an original data volume of 260.2–481.4 MB. Using the HiFi data obtained from sequencing, Flye v2.9.5-b1801 was employed for de novo whole-genome assembly [17]. The assembly results were visualized using Bandage v0.9.0 software [18]. Mitochondrial genome sequences were then extracted from the whole-genome data based on sequencing depth, sequence length, and BLAST. Genome-wide resequencing data from 25 second-generation *H. marmoreus* samples were downloaded from NCBI and assembled using GetOrganelle v1.7.7.1 [19]. The mitochondrial genomes were annotated using MFannot [20] and Mitos [21]. For codon translation, the mitochondrial genetic code molds/protozoa/coelenterates (transl_table=4) was applied in both MFannot and Mitos. The annotation results were manually corrected using Geneious v2025.0.2 software to ensure their accuracy. The annotation results were visualized using OGDRAW v1.3.1. The secondary structure was predicted using tRNAscan-SE v2.0.12 [22], a preliminary structure prediction graph was generated using RNAplot v2.7.0 [23], and finally visualized using a Python script.

2.4. Repeat Sequence Analysis

The MISA (MicroSatellite) Perl script was used to identify simple sequence repeat (SSR) loci in the mitochondrial genome sequences of all strains. Default parameters were applied, with the minimum repeat occurrences for 1-6 nt units set as 10, 6, 5, 5, 5, and 5, respectively [24]. Forward (F),

© 2025 by the author(s). Distributed under a Creative Commons CC BY license.

Preprints.org (www.preprints.org) | NOT PEER-REVIEWED | Posted: 28 February 2026 doi:10.20944/preprints202602.1502.v1

palindromic (P), reverse (R), and complementary (C) repeat sequences were detected using the REPuter online tool, with a minimum repeat size set to 30 bp and an edit distance of 0. Long tandem repeats (>6bp) were detected using the TRF online tool, with all parameters set to default values (2, 7, 7, 10, 50, and 500). All repeat sequence statistics were visualized using R language v4.3.1.

2.5. Codon Preference Analysis

Based on the mitochondrial genome annotation results of *H. marmoreus*, 15 common Protein-Coding gene (PCG) sequences were extracted using PhyloSuite v1.2.3[25]. The Relative Synonymous Codon Usage (RSCU) was calculated using MEGA v11[26], where RSCU>1 indicates that the codon was preferred for amino acids, and RSCU<1 indicates that the codon was used less frequently than expected.

2.6. Non-Synonymous and Synonymous Substitution (Ka/Ks) Analysis

The conserved PCG sequences from the mitochondrial genomes of the 31 *H. marmoreus* strains were aligned using MAFFT v7.526 [27]. Subsequently, we calculated the non-synonymous substitution rate (Ka) and synonymous substitution rate (Ks) using pamlX v1.3.1 [28]. The Ka/Ks ratio was analyzed to assess evolutionary selection pressure.

2.7. Single Nucleotide Polymorphism Analysis

Single nucleotide polymorphism (SNP) analyses was conducted at 15 PCGs levels. Multiple sequence alignments were performed on the corresponding sequences using MAFFT v7.505 software [27]. SNPs were detected using DnaSP v6 [29], and the nucleotide polymorphism (π) and Watterson's θ population genetic diversity parameters were calculated. Gene location information in the GB annotation file was read using a custom Python script, and combined with SNP data, a mitochondrial genome rearrangement pattern diagram was drawn using ggplot2 (R package).

2.8. Population Structure Analysis

Single nucleotide variant (SNV) data were screened using SNP-sites v2.5.1[30]. Population genetic structure analysis was conducted within a range of K values (2-8) using Admixture v1.3.0, and the optimal K value was determined through cross-validation [31]. The phylogenetic tree was constructed using the maximum likelihood method using IQ-TREE v2.0.7 software [32]. Model selection was automatically completed using ModelFinder, and the support rate was evaluated through 1,000 ultrafast boots (UFBoot). Visualization was performed using the iTOL online platform [33].

2.9. Mitochondrial Pan-Genome Analysis of H. marmoreus

Gene family clustering was performed on the protein sequences of the 31 strains using OrthoFinder v2.55 [34]. Based on the presence-absence patterns of gene families, simulations of the pan-genome and core genome were performed via a custom script to calculate the number and distribution of core genes, non-core genes, and private gene families across strains. To construct the high-resolution variation map of the mitochondrial pangenome of *H. marmoreus*, the mitochondrial sequence of strain f2 was used as a reference, and the Minigraph-Cactus pangenome pipeline (v2.9.3) was employed, starting with Minigraph to efficiently capture SVs and construct the initial topological framework[35]. Subsequently, progressive multi-sequence alignment was performed using Cactus v7.0.0 software to generate a comprehensive graph pan-genome file (GFA format) and the corresponding hierarchical alignment file. On this basis, the "vg call" function of vg toolkit v1.6.1.0 software was used for mutation invocation [36], and a mutation set with high confidence was obtained through quality filtering. For complex variation regions, the wavelet decomposition method was adopted to analyze multi-allelic and nested variations. Finally, bcftools v1.19 software was used to statistically analyze the variation results[37]. After construction, the mitochondrial pan-genome

© 2025 by the author(s). Distributed under a Creative Commons CC BY license.

Preprints.org (www.preprints.org) | NOT PEER-REVIEWED | Posted: 28 February 2026 doi:10.20944/preprints202602.1502.v1

map was visualized based on SV using Bandage v0.9.0 software [18], and the topological structure of the map was analyzed using ODGI v0.9.2 to evaluate its complexity and connectivity [38].

3. Results

3.1. Sequence Characteristics of the Mitochondrial Pan-Genome of H. marmoreus

Based on sequence homology with the *H. marmoreus* mitochondrial genome (GenBank: MF133443.1) [6], the mitochondrial genomes of 106,605 bp (f2) and 106,609 bp (f4) were identified in the white varieties, while those of 104,282 bp (nn12-1) and 104,284 bp (nn12-17) were identified in the brown varieties (Figure 1). All four complete mitochondrial genomes from *H. marmoreus* strains were circular DNA molecules with GC contents ranging from 31.52% to 31.72%, containing 41 to 49 annotated genes. Compared to other edible fungi, the mitochondrial genome size of *H. marmoreus* was comparable to that of *Sanghuangporus sanghuang* (112,060 bp) and *Antrodia cinnamomea* (115,207 bp), but larger than those of *Schizophyllum commune* (49,704 bp), *Pleurotus ostreatus* (65,311 bp), *Volvariella volvacea* (65,668 bp), *P. eryngii* (72,650 bp), *Hericium erinaceus* (83,518 bp), and *F. filiformis* (88,513 bp), while smaller than those of *Lentinula edodes* (121,685 bp), *A. bisporus* (135,005 bp), and *Grifola frondosa* (197,486 bp) [39]. Significant differences in mitochondrial genome size among different edible fungi may be attributed to diversity in genome structure, including variations in the number and arrangement of core genes, as well as the number and types of introns[40].

© 2025 by the author(s). Distributed under a Creative Commons CC BY license.

Preprints.org (www.preprints.org) | NOT PEER-REVIEWED | Posted: 28 February 2026 doi:10.20944/preprints202602.1502.v1

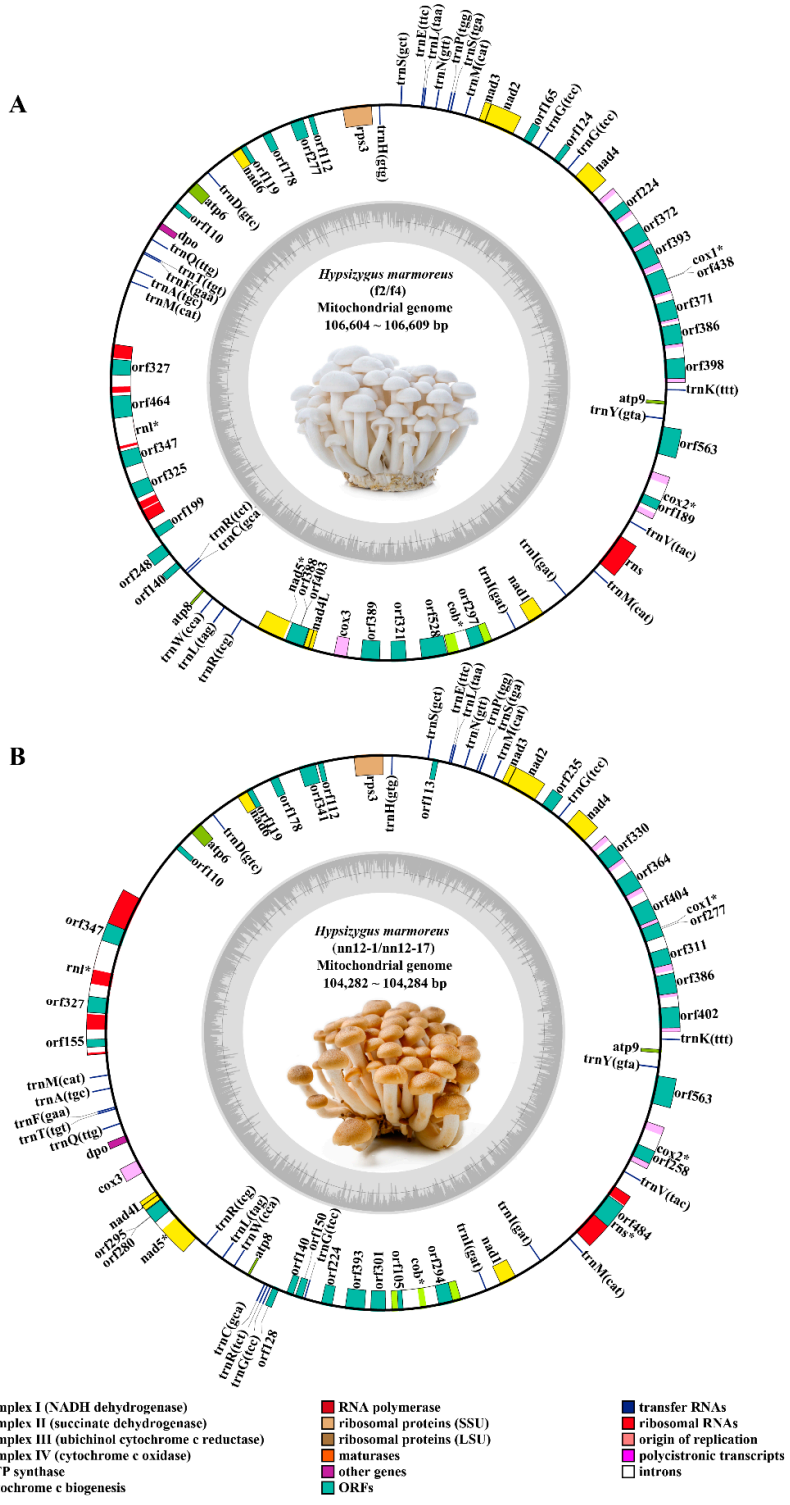

Figure 1. Mitochondrial genome map of the *H. marmoreus*. The A map represents the white *H. marmoreus*, while the B map represents the brown *H. marmoreus*. Genes displayed outside the circle are transcribed in a clockwise direction, while those inside the circle are transcribed in a counterclockwise direction. Different colors indicate different functional genes. GC content is represented by a dark gray graph on the inner circle.

Simultaneously, based on the assembly of 27 public datasets of *H. marmoreus* downloaded from NCBI, and combined with the mitochondrial genomes assembled from the four strains for joint analysis, the size range of the 31 mitochondrial genomes was found to be 98,284 bp to 111,087 bp,

© 2025 by the author(s). Distributed under a Creative Commons CC BY license.

Preprints.org (www.preprints.org) | NOT PEER-REVIEWED | Posted: 28 February 2026 doi:10.20944/preprints202602.1502.v1

with GC content ranging from 31.52% to 32.12%. They contained 39 to 49 annotated genes (Table 1). A total of 15 conserved PCGs were identified in the mitochondrial genomes of the 31 strains. These genes play important functions in the electron transport chain and oxidative respiration, including seven NADH dehydrogenase-coding genes (*nad1*, *nad2*, *nad3*, *nad4*, *nad4L*, *nad5*, and *nad6*). The mitochondrial genomes also contained the following genes: a gene encoding a subunit of complex III (ubiquinol–cytochrome c reductase), one cytochrome b–encoding gene (*cob*); three cytochrome c oxidase genes (*cox1*, *cox2*, and *cox3*) involved in the respiratory electron transport chain; three ATP synthase subunit-coding genes (*atp6*, *atp8*, and *atp9*); and one ribosomal protein S3-coding gene (*rps3*). In addition, during re-annotation of the 31 *H. marmoreus* mitochondrial genomes, a DNA polymerase-coding gene (*dpo*) was identified in 27 strains, whereas it was not detected in the remaining four strains, indicating the existence of a strain-specific deletion. These results indicate that there are significant intraspecific variations in the size and number of genes of the mitochondrial genome of *H. marmoreus*, providing a basis for subsequent exploration of its structural dynamics and evolutionary mechanisms. These significant intraspecific variations in mitochondrial genome size and gene number provide important genetic basis for germplasm classification and genetic diversity evaluation of *H. marmoreus*.

© 2025 by the author(s). Distributed under a Creative Commons CC BY license.

Table 1. Summary of mitochondrial genome assembly characteristics of 31 *H. marmoreus* strains.

Number	Name of Species	Size（bp）	Introns	Exons	Total Genes	Genes for Protein Coding	No. of rRNA	No. of tRNA	GC Contents %	Accession No.	Source information
1	*H. marmoreus*	104,282	10	14	78	48	2	28	31.52	nn12-1	This study
2	*H. marmoreus*	104,284	10	14	74	46	2	28	31.52	nn12-17	
3	*H. marmoreus*	106,605	10	14	75	47	2	27	31.72	f2	
4	*H. marmoreus*	106,609	10	14	76	47	2	27	31.72	f4	
5	*H. marmoreus*	98,284	7	9	65	39	2	28	31.75	SRR7874787	[2]
6	*H. marmoreus*	102,752	9	13	72	44	2	27	31.86	MH382825.1	[6]
7	*H. marmoreus*	106,518	10	14	77	49	2	27	31.67	MF133443.1	
8	*H. marmoreus*	106,608	10	14	75	47	2	27	31.72	SRR8699805	
9	*H. marmoreus*	106,718	10	14	75	47	2	27	31.77	SRR8699833	
10	*H. marmoreus*	105,706	10	14	74	47	2	25	31.64	SRR8699796	
11	*H. marmoreus*	106,610	10	14	75	47	2	27	31.72	SRR8699803	
12	*H. marmoreus*	106,773	10	14	75	47	2	27	31.75	SRR8699801	
13	*H. marmoreus*	106,699	10	14	76	48	2	27	31.77	SRR8699802	
14	*H. marmoreus*	106,677	10	14	75	47	2	27	31.75	SRR8699837	
15	*H. marmoreus*	106,604	10	14	75	47	2	27	31.72	SRR8699817	
16	*H. marmoreus*	106,606	10	14	75	47	2	27	31.73	SRR8699808	
17	*H. marmoreus*	106,608	10	14	75	47	2	27	31.72	SRR8699813	
18	*H. marmoreus*	106,711	10	14	76	48	2	27	31.75	SRR8699800	
19	*H. marmoreus*	106,612	10	14	76	48	2	27	31.73	SRR8699835	
20	*H. marmoreus*	106,699	10	14	75	47	2	27	31.74	SRR8699816	
21	*H. marmoreus*	106,691	10	14	75	47	2	27	31.75	SRR8699834	

© 2025 by the author(s). Distributed under a Creative Commons CC BY license.

22	*H. marmoreus*	106,609	10	14	75	47	2	27	31.72	SRR8699814	
23	*H. marmoreus*	106,620	10	14	75	47	2	27	31.73	SRR8699815	
24	*H. marmoreus*	105,589	10	14	74	48	2	25	31.61	SRR8699809	
25	*H. marmoreus*	106,609	10	14	69	41	2	27	31.72	SRR8699804	
26	*H. marmoreus*	106,603	10	14	75	47	2	27	31.72	SRR8699797	
27	*H. marmoreus*	106,602	10	14	69	41	2	27	31.72	SRR8699811	
28	*H. marmoreus*	111,087	9	12	74	46	2	27	32.12	SRR12151860	[4]
29	*H. marmoreus*	106,670	10	14	75	47	2	27	31.74	SRR12151875	
30	*H. marmoreus*	111,031	9	12	75	47	2	27	32.11	SRR12151871	
31	*H. marmoreus*	111,037	9	12	74	46	2	27	32.11	SRR12151883	

© 2025 by the author(s). Distributed under a Creative Commons CC BY license.

Preprints.org (www.preprints.org) | NOT PEER-REVIEWED | Posted: 28 February 2026 doi:10.20944/preprints202602.1502.v1

3.2. Secondary Structure Analysis of tRNAs in the Mitochondrial Genome of H. marmoreus

tRNAs are key for deciphering the genetic code of mRNA and mediating protein synthesis. The typical cloverleaf-shaped structure conforms to the conserved characteristics of mitochondrial tRNA, and the additional spherical structure expands the conformational spectrum of mitochondrial tRNA. In this study, the mitochondrial genomes of the 31 strains were found to contain 25-28 tRNAs, mainly composed of 22 core tRNAs and some of their replicas, collectively responsible for the transport of 20 amino acids (Figure 2). The secondary structure prediction results showed that 14 tRNA molecules presented typical cloverleaf structures, while 5 tRNAs (tRNA-Leu1, tRNA-Leu2, tRNA-Ser1, tRNA-Ser2, and tRNA-Tyr) had expanded ring structures at the DHU or TΨC ring. Three tRNAs (tRNA-Thr, tRNA-Trp, and tRNA-Glu) presented atypical, elongated arms or long-strip conformations. Copy number analysis indicated that tRNA-Met had three copies in all strains, tRNA-Gly had two copies in most strains but three copies in the nn12-1 and nn12-17 strains. These results revealed significant diversity in the secondary structure and copy number of tRNAs in the mitochondria of *H. marmoreus*, suggesting that it may be related to adaptive evolution or functional differentiation processes.

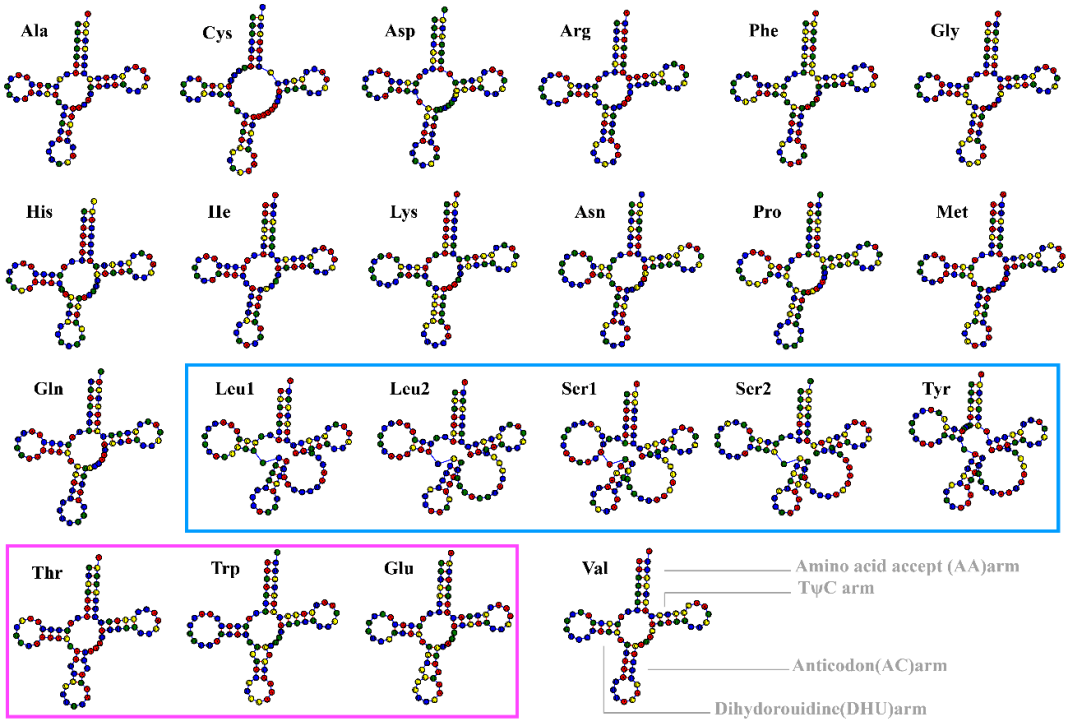

Figure 2. tRNA secondary structure prediction map of the 20 amino acids encoded by the mitochondrial genome of *H. marmoreus*. The red, blue, green, and yellow spheres represent the bases A, U, G, and C, respectively. The blue and purple boxes denote different types of variants.

3.3. Analysis of Repeat Sequence Characteristics in the Mitochondria of H. marmoreus

Investigating the characteristics of mitochondrial repetitive sequences in *H. marmoreus* helped to reflect evolutionary selection preferences for different repeat types, elucidate their genetic mechanisms, and facilitate germplasm resource identification. This study employed SSR detection, REPuter, and TRF software to conduct a systematic analysis of various repetitive sequence types within the mitochondria of 31 *H. marmoreus* strains.

SSR detection successfully revealed eight different SSR motifs (Figure 3A), including two mononucleotide SSRs, one dinucleotide SSR, one trinucleotide SSR, one tetranucleotide SSR, one pentanucleotide SSR, and two hexanucleotide SSRs. Among them, C/G motif variants were the most

© 2025 by the author(s). Distributed under a Creative Commons CC BY license.

Preprints.org (www.preprints.org) | NOT PEER-REVIEWED | Posted: 28 February 2026 doi:10.20944/preprints202602.1502.v1

abundant, and the quantity varied significantly among strains (SRR7874787 contained 38, while MF133443.1 and MH382825.1 had only 29). The abundance of A/T-type motifs was the second highest (average 24.4). Notably, tetranucleotide motifs (AAAT/ATTT) were present in only three samples, and pentanucleotide motifs (AAATT/AATTT) were found in only four samples, all as single copies. The enrichment of C/G motifs appears to be a common feature of the mitogenomes of edible fungi. For instance, in *L. edodes*, C/G-type SSRs account for over 60% of total SSRs, and variations in their tandem repeats have been linked to evolutionary pathways and nuclear-cytoplasmic compatibility [41]. Similarly, a large-scale pan-mitogenome study of 361 *A. bisporus* strains demonstrated that a high frequency of C/G motifs correlated positively with genomic stability, potentially because they formed stronger hydrogen bonds, thereby contributing to DNA duplex stability [13].

Analysis using REPuter software revealed significant differences in the abundances of four types of repetitive sequences-forward (F), palindromic (P), reverse (R), and complementary (C)-within the mitochondrial genome of *H. marmoreus*. These sequences exhibited the following distribution pattern: F > P > R > C (Figure 3B). At the individual sample level, the abundance of each repeat type varied markedly among strains. Notably, sample SRR8699801 contained only nine palindromic repeats (P), which was significantly below the average across all samples, whereas its reverse repeats (R) reached 16 occurrences, which was markedly higher than the reverse repeat frequency observed in all other samples.

Long tandem repeat sequences ranging from 20 to 100 bp were identified using TRF software. The results showed that repeat sequences of different length ranges presented different distribution patterns in the mitochondria of *H. marmoreus* (Figure 3C). Among all samples, the content of repeat sequences with a length of 41-50 bp was the highest, with an average of 10.2 repeats, and this length reached 11 repeats in 21 samples. The abundance of repeat sequences with a length of 20-30 bp ranked second, with an average of 5.5 repeats. Moreover, among the 26 samples, the number of repeats was relatively high, reaching 6 repeats. Notably, in the 71-90 bp length range, no repeat sequences were found in any of the samples. In the 91-100 bp length range, only two strains, nn12-1 and nn12-17, each contained one repeat. No repeat sequences within this range were detected in the remaining samples. In conclusion, the mitochondrial repeat sequences of *H. marmoreus* showed a high degree of polymorphism in type, abundance, and distribution. The dynamic changes in these repeat elements may be one of the important forces driving genome size variation and structural evolution. The high polymorphism of mitochondrial repetitive sequences in *H. marmoreus* can be used as molecular markers for germplasm identification and genetic diversity analysis of this species.

© 2025 by the author(s). Distributed under a Creative Commons CC BY license.

Preprints.org (www.preprints.org) | NOT PEER-REVIEWED | Posted: 28 February 2026 doi:10.20944/preprints202602.1502.v1

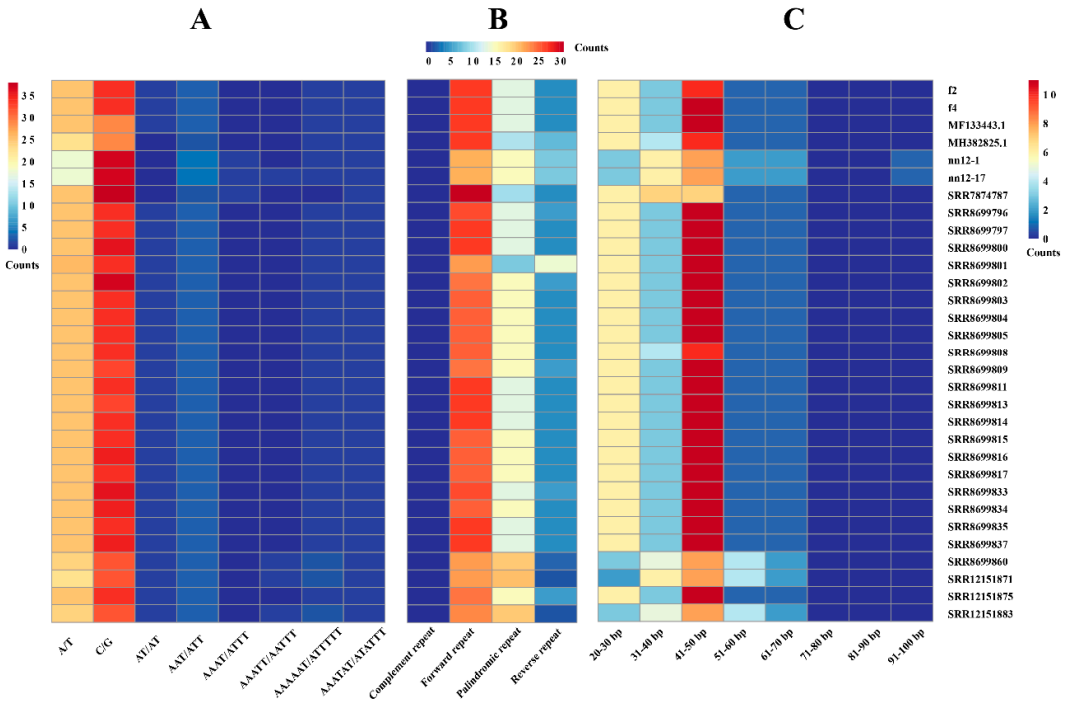

Figure 3. Heatmap of annotated repetitive sequences in the mitochondrial genome of *H. marmoreus*. (A) Eight SSR motifs detected; (B) Interspersed repeat; (C) Long tandem repeat sequences, ranging from 20 bp to 100 bp, with increments of 10 bp.

3.4. Analysis of Codon Usage Preferences in the Mitochondrial Genome of H. marmoreus

The codons in the mitochondrial genome of *H. marmoreus* were analyzed using RSCU, and a significant bias was found in the use of synonymous codons for most amino acids (Figure 4). From the perspective of amino acid codon preference, UUU (RSCU=1.45) for phenylalanine and AUU (RSCU=1.29) for isoleucine were used more frequently, reflecting a preference for U at the third codon position. AGA (RSCU=4.98) for arginine, UUA (RSCU=3.53) for leucine, and AAA (RSCU=1.70) for lysine were also used more frequently, indicating a preference for A at the third codon position. Furthermore, the dominant codons of most amino acids, such as proline, valine, and threonine, reflected a strong A/T base preference in the mitochondrial genome, which is consistent with previous findings that the mitochondrial PCG synonymous codons in eight *Pleurotus* strains also preferred to end with A/T [42].

© 2025 by the author(s). Distributed under a Creative Commons CC BY license.

Preprints.org (www.preprints.org) | NOT PEER-REVIEWED | Posted: 28 February 2026 doi:10.20944/preprints202602.1502.v1

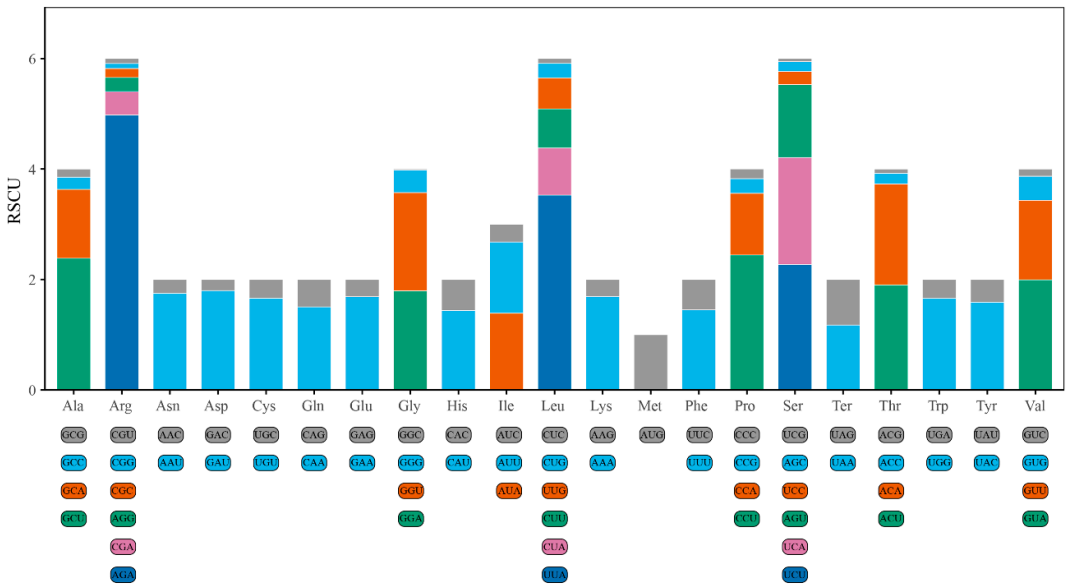

Figure 4. Relative synonymous codon usage (RSCU) analysis of the mitochondrial genome of *H. marmoreus*.

3.5. Analysis of Substitution Rates in the Mitochondrial PCGs of H. marmoreus

The Ka/Ks ratio was used to show the differences in evolutionary constraints for 15 conserved PCGs of 31 *H. marmoreus* strains (Figure 5). The ω values of *cox1*, *cob*, *nad2*, *nad3*, *nad4L*, *nad5*, and *rps3* ranged between 0 and 1, while the remaining eight genes exhibited values close to 0 (ω≈0), indicating that purifying selection is the dominant force in the evolution of these core genes. The *cox1* (ω=0.131) and *cob* (ω=0.123) genes, which encode cytochrome c oxidase subunit I and cytochrome b, respectively, showed strong evolutionary conservation. This is consistent with the essential requirement for a stable and efficient respiratory chain to support mycelial growth and fruiting body development in *H. marmoreus*, a wood-decaying fungus that relies on lignocellulose decomposition for energy. The genes *nad2* (ω=0.049), *nad3* (ω=0.278), *nad4L* (ω=0.561), and *nad5* (ω=0.06), which encode subunits of the mitochondrial NADH dehydrogenase complex, also exhibited low Ka/Ks ratios. This complex is crucial for electron transfer in the respiratory chain, and even minor amino acid changes disrupt its structure and impair energy production, suggesting strong purifying selection. Furthermore, *atp8* and *cox3* were completely conserved across all 31 strains, whereas *atp6*, *atp9*, *nad1*, *nad4*, and *nad6* only contained synonymous substitutions. Collectively, these patterns indicated intense purifying selection and high functional constraints. This finding is consistent with findings in other basidiomycetes, where the overall Ka/Ks values of 14 core PCGs in five *Ganoderma* species [43] and five *Boletus* species [44] were also below 1, confirming that purifying selection is the dominant evolutionary force acting on essential mitochondrial respiratory genes.

© 2025 by the author(s). Distributed under a Creative Commons CC BY license.

Preprints.org (www.preprints.org) | NOT PEER-REVIEWED | Posted: 28 February 2026 doi:10.20944/preprints202602.1502.v1

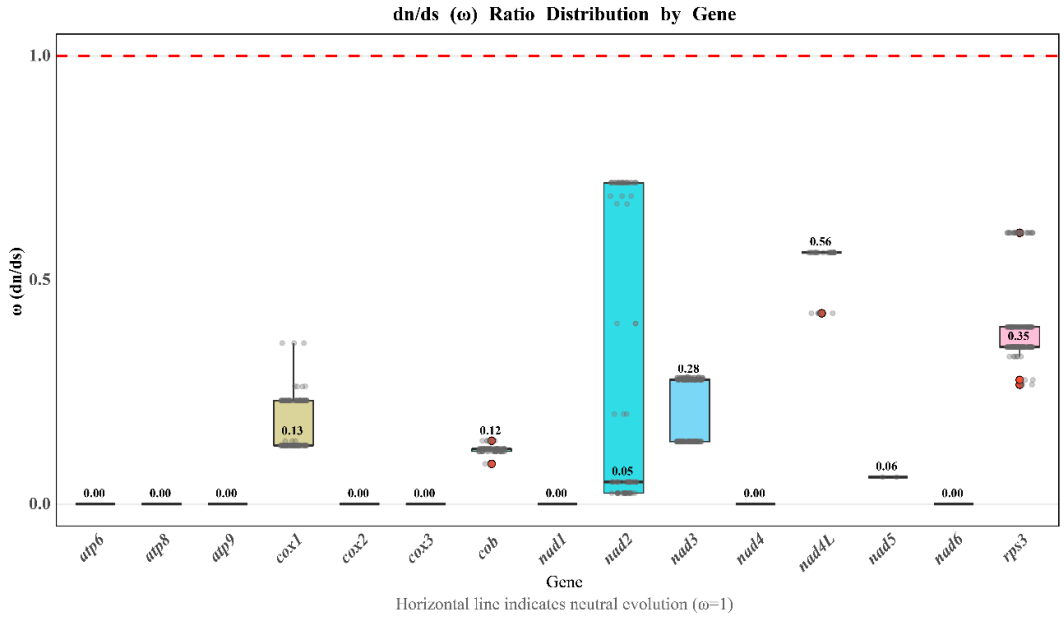

Figure 5. Selective pressure analysis of 15 core protein-encoding genes in the mitochondrial genomes of 31 *H. marmoreus* strains.

3.6. Analysis of Nucleic Acid Diversity in the Mitochondria of H. marmoreus

Analysis of the core genes revealed low nucleotide diversity (Pi < 0.03) across most of them (Figure 6A), with only the *nad2* gene showing a relatively higher value. This indicates that the core functions of the respiratory chain are subject to intense purifying selection, while genes and non-coding sequences exhibit distinct evolutionary rates. In the mitochondrial genomes of 31 *H. marmoreus* strains, we observed large-scale structural rearrangements driven by two major molecular events (Figure 6B). Event A is a 18,535 bp IR-mediated inversion involving the *nad2–nad3–rps3* region, mediated by a pair of 385 bp inverted repeats (IR) with 88.1% identity, occurring in 38.7% of the strains. Event B is a 12,171 bp inversion of the *atp8–nad5–nad4L–cox3* region, occurring in 16.1% of strains. In the reference genome (f2), a pair of 265 bp direct repeats (DR, 90.6% identity) flank the *dpo* and *cox3* regions. In inverted strains, these dispersed repeats have evolved into a 213 bp inverted repeat pair (IR, 92.0% identity), which subsequently mediated the segmental inversion through intramolecular homologous recombination. Based on gene arrangement patterns, we classified the 31 strains into 8 distinct gene orders (Figure 6C), including 6 core rearrangement patterns and 2 cases caused by tRNA loss. Pattern 1 represents the reference type (Ref.f2), containing 14 strains; Pattern 2 corresponds to Event A inversion (11 strains); Pattern 3 is a combination of Event B and *rnl* inversion (2 strains); Pattern 4 is a variant of Event B (2 strains); Pattern 5 is a combined inversion of Event A and B (1 strain); Pattern 6 is *rnl* inversion alone (1 strain); Patterns 7 and 8 represent *trnL/E* loss combined with Event A or the reference type, respectively (1 strain each). These patterns suggest that mitochondrial genome rearrangements may enhance adaptability by altering gene expression patterns or generating new gene combinations. The identified genetic variation hotspots and conserved regions provide candidate sites for the development of molecular markers for *H. marmoreus* molecular breeding.

© 2025 by the author(s). Distributed under a Creative Commons CC BY license.

Preprints.org (www.preprints.org) | NOT PEER-REVIEWED | Posted: 28 February 2026 doi:10.20944/preprints202602.1502.v1

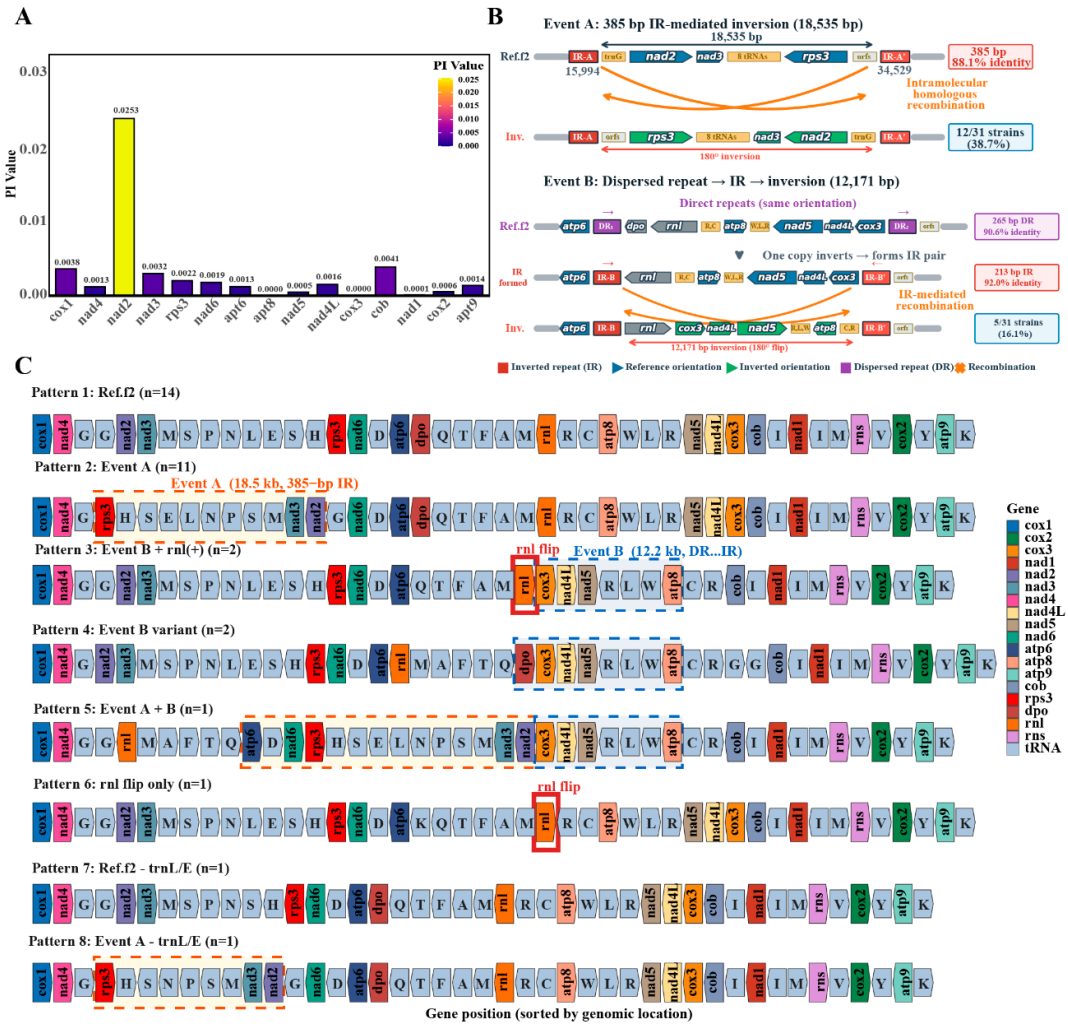

Figure 6. Analysis of nucleic acid diversity in the mitochondrial genome of *H. marmoreus*. (A) Analysis of nucleotide polymorphisms at the PCG gene level (window length 100 bp, step size 25 bp); (B)Two major molecular events driving large-scale structural rearrangements in the mitochondrial genome of *H. marmoreus*; (C) Eight unique gene arrangement patterns identified in 31 strains of *H. marmoreus*. The different colors in the figure represent different genetic types. Among them, the light blue blocks represent the single-letter abbreviations encoded by various tRNAs.

3.7. Phylogenetic and Population Structure Analysis of H. marmoreus

Based on SNP data from 31 mitochondrial genomes of *H. marmoreus*, we determined its population structure characteristics. ADMIXTURE analysis showed that when K=5, the cross-validation error was the lowest (Figure 7A), indicating that K=5 was the optimal clustering level for the SNP matrix. This result suggested that the samples could be divided into five major genetic clusters (Figure 7B). Among them, the genetic backgrounds of clusters C1, C2, and C3 were relatively pure, whereas some individuals in clusters C4 and C5, such as the SRR12151860 strain, showed mixed genetic components derived from multiple ancestral groups. Phylogenetic tree analysis further supported this classification, with a relatively high bootstrap support rate (>95%) among the different branches, suggesting that these lineages have undergone relatively independent genetic drift and fixation events during their evolutionary history (Figure 7C). The five genetic clusters and obvious population differentiation provide a theoretical basis for the selective breeding and germplasm innovation of *H. marmoreus*.

© 2025 by the author(s). Distributed under a Creative Commons CC BY license.

Preprints.org (www.preprints.org) | NOT PEER-REVIEWED | Posted: 28 February 2026 doi:10.20944/preprints202602.1502.v1

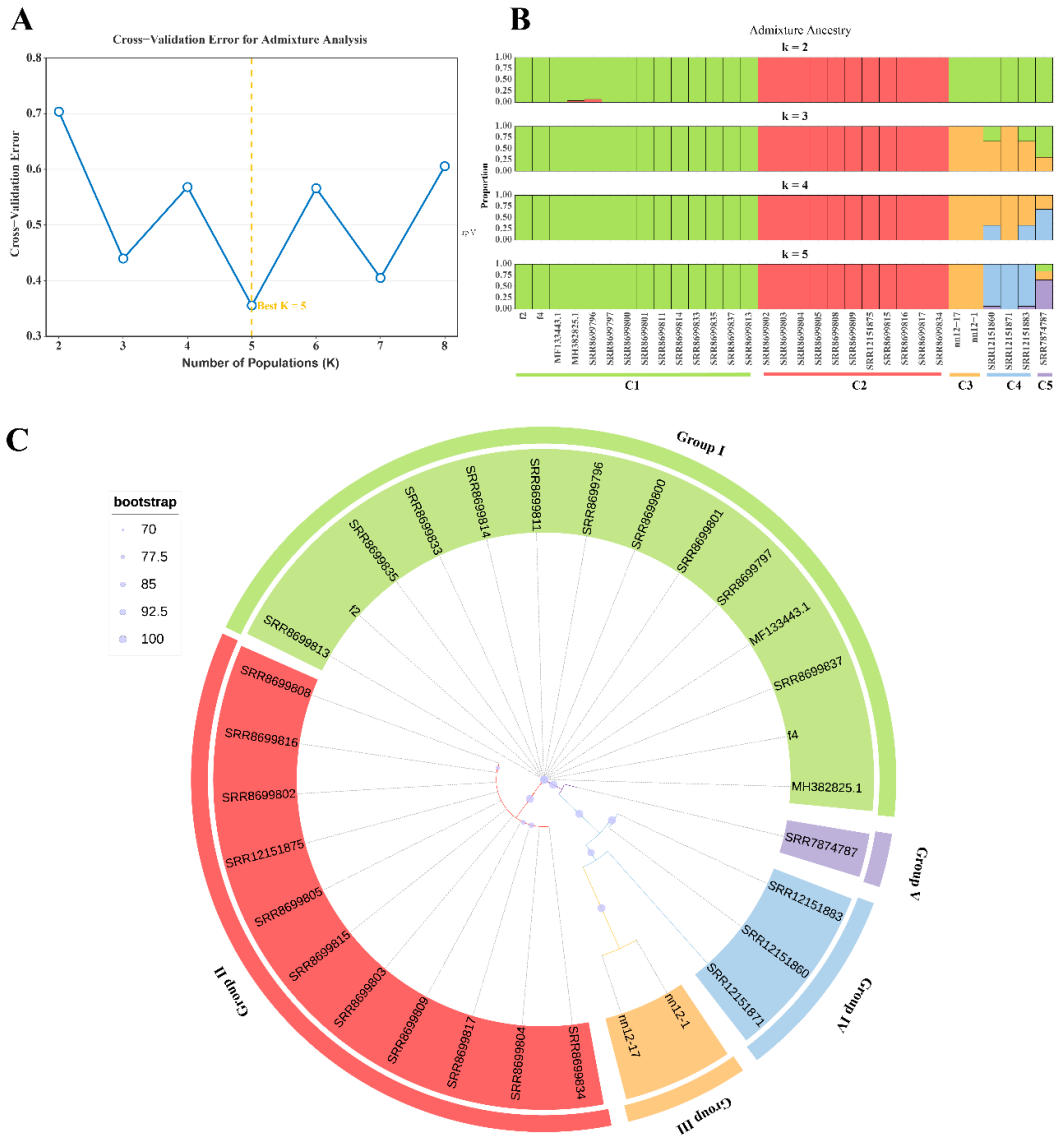

Figure 7. Phylogenetic and population structure analysis of *H. marmoreus*. (A) Cross-validation error from ADMIXTURE analysis; (B) Population structure bar plots at K=2 to 5; (C) Phylogenetic tree based on mitochondrial genomic SNPs.

3.8. Analysis of the Pan-Genome of the Mitochondrial DNA of H. marmoreus

The pan-genome population growth curve showed that when the number of strains increased to approximately 25–28, the pan-genome entered a plateau phase (power-law fit: $y=46.48 \times x^{0.087}$ ($B < 1$)), indicating that the pan-genome of this species tends to be near-closed (Figure 8A). Based on the frequency of gene families across the 31 genomes, a total of 62 gene clusters were identified and classified into four categories: core genes (26, accounting for 41.9%), softcore genes (4, 6.5%), dispensable genes (30, 48.4%), and unique genes (2, 3.2%) (Figure 8B) [45]. In previous studies, differences in mitochondrial genome size were mainly associated with intron insertion polymorphisms, repetitive sequences, and large-fragment SVs. In *H. marmoreus*, the mitochondrial genome sizes were mainly distributed in three intervals: 98 kb, 102-106 kb, and 111 kb (Figure 8C). Further analysis revealed that among the 31 strains, there were significant differences in the number of introns in four genes, *cox1*, *nad5*, *cox2*, and *cob*. Among these, the *cox1* gene contained the largest number of introns, with most strains harboring seven introns. However, the *cob* and *cox2* genes of

© 2025 by the author(s). Distributed under a Creative Commons CC BY license.

Preprints.org (www.preprints.org) | NOT PEER-REVIEWED | Posted: 28 February 2026 doi:10.20944/preprints202602.1502.v1

SRR7874787 contained no introns. The genome of this strain was the shortest among all strains, which is consistent with a significant association between intron deletions and genome length (Figure 8D).

Analysis based on orthologous groups revealed that non-core variable genes exhibited pronounced presence–absence variation (PAV) among different strains (Figure 8E), indicating heterogeneous conservation patterns across the mitochondrial pan-genome. Specifically, orf563, orf297/294, and orf321 were highly conserved and remained stable in the majority of strains (28–29 out of 31), whereas orf113, orf128, orf114, and orf301 were detected only sporadically in 2–3 strains, reflecting their strain-specific distribution. Notably, the *dpo* gene, encoding a DNA polymerase derived from mitochondrial plasmid integration, was absent in the four strains that experienced IR-mediated genome rearrangements (SRR12151860, SRR12151871, SRR12151883, and SRR7874787), suggesting a potential association between large-scale structural variation and the loss of plasmid-derived sequences. In addition, several ORFs (including orf128, orf140, and orf301) were exclusively present in the nn12-1 and nn12-17 strains and localized to intergenic regions, implying rapid evolutionary dynamics that may contribute to mitochondrial genome diversification and functional differentiation.

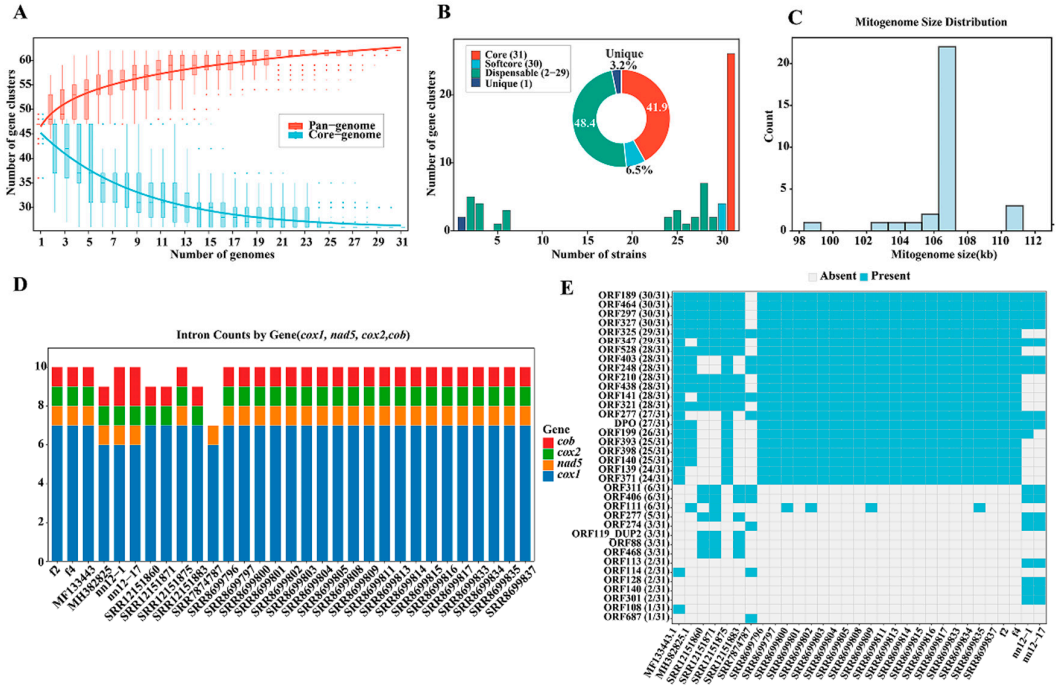

Figure 8. Analysis of mitochondrial pan-genome and structural variation characteristics of *H. marmoreus*. (A) Profiling of the mitochondrial pan-gene pool; (B) Distribution of gene families and composition of core, soft-core, accessory, and strain-specific genes across the 31 mitogenomes; (C) Variation in genome length among the 31 strains; (D) Distribution of intron numbers in the *cox1*, *nad5*, *cox2*, and *cob* genes across the 31 strains; (E) Presence-absence variation (PAV) profile of genes in the 31 *H. marmoreus* mitogenomes. The blue square indicates the presence of the corresponding homologous gene in the specific strain.

Based on 31 mitochondrial genomes of *H. marmoreus*, we successfully constructed a mitochondrial pattern pan-genome using the f2 strain as the reference. This pan-genome was generated in graphic fragment assembly (GFA) format, with a total length of 220,364 bp, containing 217 nodes and 293 edges. The overall structure reflects the SV characteristics of the mitochondrial genome. BLAST localization analysis of core coding genes revealed that most core gene regions did not undergo significant SV, whereas genes containing introns exhibited large-fragment insertions/deletions (Figure 9A). Specifically, the *cox1* gene region exhibits multiple bubble-like structures, mainly due to intron insertion and deletion events. Among the 31 strains of *H. marmoreus*,

© 2025 by the author(s). Distributed under a Creative Commons CC BY license.

Preprints.org (www.preprints.org) | NOT PEER-REVIEWED | Posted: 28 February 2026 doi:10.20944/preprints202602.1502.v1

27 strains (87.1%) maintained the canonical "7 introns + 8 exons" structure of the *cox1* gene, including 24 strains sharing identical intron insertion sites with the reference strain f2 and three rearranged strains (SRR12151860, SRR12151871, and SRR12151883) in which the seven introns were retained but positioned at partially different locations. The *nad5* gene was simultaneously affected by both gene rearrangement and intron variation. Sequence analysis revealed that 26 strains (83.9%) maintained the canonical antisense *nad5* arrangement carrying a 1,363 bp intron. Two rearranged strains (nn12-1 and nn12-17) retained the intron (1,447 bp) despite sense-strand inversion, whereas three rearranged strains (SRR12151860, SRR12151871, and SRR12151883) exhibited both orientation disruption and complete intron loss. The *cob* gene contained a single intron in 28 strains (90.3%), whereas nn12-1 and nn12-17 acquired an additional intron at position 820 site, and SRR7874787 lacked introns entirely. The *cox2* gene carried a single intron in 30 strains (96.8%), with substantial length variation among strains. Aside from the genes described above, no large-scale structural variations were detected in other mitochondrial coding regions.

In addition, 2,323 variant sites were identified, including 1,563 SNPs, 522 insertions and deletions (InDels), 246 polynucleotide polymorphisms (MNPs), and 175 other complex variations (Figure 9Ba). The conversion to transmutation ratio was 820:690 (1.19:1), which was relatively low but conformed to the common conversion bias characteristics of the mitochondrial genome, reflecting the high spontaneous mutation tendency of mitochondrial DNA (Figure 9Bb). The InDels analysis results showed that short fragment InDel events (≤5 bp) dominated. In total, 186 single-base deletions (-1) and 144 single-base insertions (+1) were detected. Variations were mainly distributed in the intergenic regions, followed by the coding regions. However, the variation density (number of variations per kb) in the rRNA region was slightly higher than that in the CDs region (Figure 9C). Specifically, C>T (239 times) and G>A (197 times) were the main mutation types, followed by A>G (187 times) and T>C (197 times) (Figure 9D), which was consistent with the typical mutation pattern caused by cytosine deamination rather than mutations resulting from external DNA damage or artificial mutagenesis [46]. In addition, multiple large-fragments deletions were identified. For instance, 18 sites with 60-bp deletions were detected, suggesting the presence of structurally unstable regions in the mitochondrial pan-genome. The constructed graph-based mitochondrial pan-genome and identified abundant genetic variations provide a comprehensive genomic resource for the molecular regulation and stress-resilient variety breeding of *H. marmoreus*.

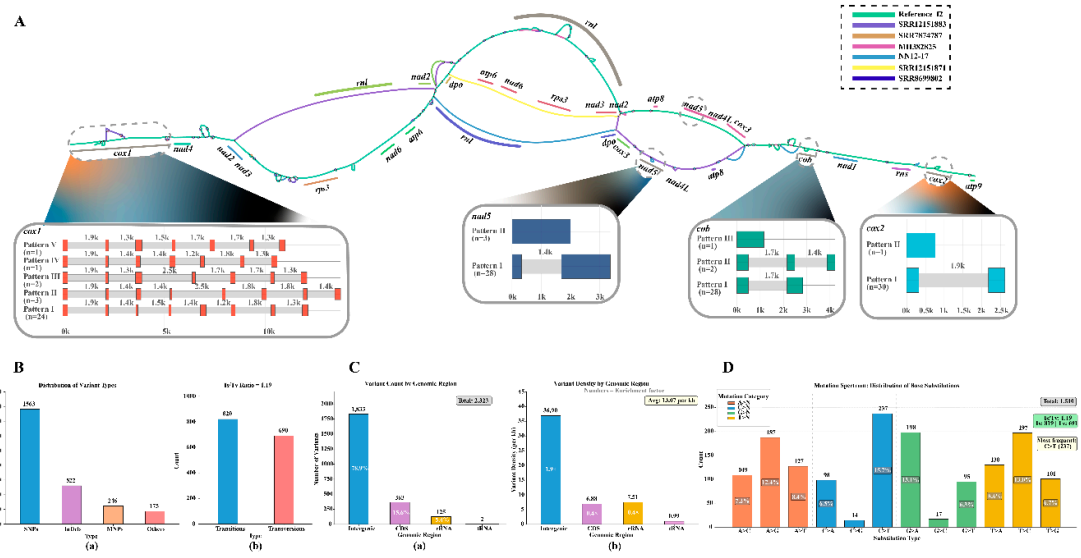

Figure 9. Analysis of the pan-genome and structural variation characteristics of the mitochondrial genome of *H. marmoreus*. (A) Construction of the mitochondrial pattern pan-genome of *H. marmoreus* based on Bandage software, where the red arrow indicates the direction of the gene sequence; (B) Classification of variation types

© 2025 by the author(s). Distributed under a Creative Commons CC BY license.

Preprints.org (www.preprints.org) | NOT PEER-REVIEWED | Posted: 28 February 2026 doi:10.20944/preprints202602.1502.v1

and the proportion of transformation and transmutation; (C) Proportion of variation occurrence across genomic regions and the variation coefficient diagram; (D) Mutation type diagram. 4. Discussion.

In this study, mitochondrial genomes from four mononuclear strains of *H. marmoreus* were sequenced and assembled, and together with publicly available NCBI datasets, a total of 31 mitochondrial genomes were integrated to construct a mitochondrial pan-genome map of *H. marmoreus*. Unlike previous mitochondrial studies of edible fungi, such as *F. filiformis* and *A. bisporus*, which were based on the assembly of a single or multiple strains, the graphical mitochondrial pan-genome generated here provides a more systematic and comprehensive analysis of mitochondrial structural diversity, intron dynamics, population structure, and evolutionary trends.

Throughout evolution, the mitochondrial genomes of animals, fungi, and plants have diverged significantly. Animal mitochondrial genomes exhibit highly conserved structures with stable gene orders but elevated point mutation rates [47], whereas plant mitochondrial genomes display extremely low point mutation rates yet high structural variability [48]. The evolutionary characteristics of fungal mitochondria lie between these two extremes, with relatively conserved coding genes but substantial variation in genome structure and size [49]. Previous studies have shown that fungal mitochondrial genomes are among the most variable groups of eukaryotes, primarily due to factors such as dynamic intron changes, accumulation of repetitive sequences, and the presence of non-conservative PCGs [50–52]. In this study, variations in the mitochondrial genome size of *H. marmoreus* (98,284–111,087 bp) were found to primarily stem from intron acquisition and loss, variations in repetitive sequences, and insertion or deletion of *dpo* genes, which provide the structural basis for subsequent rearrangement patterns. Studies have shown that dpo sequences derived from linear plasmids are often integrated into mtDNA, with insertion sites frequently located in genomic rearrangement hotspots. This is consistent with our observations in the *nad2–rps3* (Event A) and *atp8–cox3* (Event B) regions. These integrations are closely associated with genomic expansion and repetitive sequence enrichment; crucially, our results confirm that the enriched inverted repeats (IRs) act as the primary drivers of large-scale structural rearrangements via intramolecular homologous recombination[53]. Furthermore, studies in *Agrocybe aegerita* have shown that the *polB* gene may originate from linear mitochondria and, after integration, promote SVs such as local duplication or inversion [54]. These results are consistent with the gene presence/absence polymorphisms and rearrangement phenomena observed in the mitochondria of Basidiomycetes, suggesting that IR-mediated recombination, potentially triggered by the insertion of plasmid-derived mobile elements, is a key mechanism driving structural heterogeneity and rearrangement in basidiomycete mitochondria.

Most eukaryotic ancestors obtained their mitochondrial genomes from *Alphaproteobacteria* through an endosymbiotic mechanism. In subsequent evolution, most mitochondrial genes gradually integrated into the nuclear genome, retaining only a set of core and non-conserved PCGs to maintain the stability of the oxidative phosphorylation process[55]. Among the 31 *H. marmoreus* strains studied, all mitochondrial genomes contained 15 PCGs. These genes exhibited a distinct preference for A/T-terminating codons in amino acid usage, consistent with the codon preference patterns observed in the genus *pleurotus* [42]and wild *Auricularia villosula* [56]. This provides a basis for optimizing the codons of exogenous functional genes in genetic engineering breeding, enhances the expression efficiency of exogenous genes, and accelerates the breeding process of *H. marmoreus*. The Ka/Ks analysis showed that these genes have all undergone strong purification selection ($\omega<1$) during evolution, consistent with reports of some genera such as *Ganoderma* and *Boletus* [57], indicating the key role of these conserved genes in mitochondrial energy metabolism. Notably, the *nad4L* ($\omega=0.56$) and *rps3* ($\omega=0.35$) genes exhibit relatively high evolutionary rates, a phenomenon potentially linked to their relaxed functional constraints and interactions with mobile genetic elements. *nad4L* encodes a small subunit of respiratory complex I, which tends to accumulate neutral mutations more readily than core subunits, resulting in a relatively higher evolutionary rate. *rps3* is a structural component of the small subunit of mitochondrial ribosomes; however, studies have indicated that during *L.*

© 2025 by the author(s). Distributed under a Creative Commons CC BY license.

Preprints.org (www.preprints.org) | NOT PEER-REVIEWED | Posted: 28 February 2026 doi:10.20944/preprints202602.1502.v1

edodes color transformation, it may participate in regulating non-ribosomal functions such as oxidative stress responses, energy metabolism coordination, and extracellular matrix remodeling. This suggests that, while maintaining fundamental translational functions, *rps3* may also play a regulatory role in environmental adaptation [10]. These genes with higher evolutionary rates accumulate neutral mutations, making them important candidate genes for genetic improvement of agronomic traits in *H. marmoreus*, such as stress tolerance and yield.

In this study, we constructed a graphical pan-genome of the *H. marmoreus* mitochondria, revealing abundant genetic variation (including SNPs, InDels, and SVs). Compared to a linear reference genome, this approach demonstrated significant advantages in variant detection, clearly illustrating large-scale SVs and intron insertion/deletion events within the *H. marmoreus* mitochondria. Notably, the respiratory chain-related gene *cox1* exhibited significant intronic polymorphisms. Such genes are widely reported as "high-frequency carriers" of intron insertions in *Lycoperdaceae*, *L. edodes*, *P. ostreatus*, *Armillaria*, and *F. filiformis* [12]. The number and types of introns in these genes far exceed those in other PCGs [58], suggesting that the *cox1* region has a greater capacity for intron accommodation, maintenance, and loss during the evolution of fungal mitochondrial genomes. Notably, most introns in the mitochondrial genome of *H. marmoreus* were identified as Group I self-splicing endonuclease genes (HEGs). Their primary function involves homing endonucleases that cleave at homologous sites where introns are deleted, facilitating "homing" through the host DNA repair system. This process promotes the diffusion and maintenance of introns within populations and is accompanied by a series of sequence remodeling events, including local duplication, intergenic region expansion, and recombination of adjacent ORFs, thereby amplifying mitochondrial genomic structural diversity [59]. Previous studies have demonstrated that, in various basidiomycetes, Group I introns rich in HEGs are frequently associated with significant structural rearrangements and segmental insertions/deletions. This leads to marked differentiation among strains in terms of mitochondrial genome size, configuration, and gene linkage patterns [60]. These HEG-driven intronic dynamics and structural variations indirectly regulate mitochondrial energy metabolism and stress response capabilities, thereby influencing strain growth rates and stress tolerance. For the molecular regulation of *H. marmoreus* cultivation, the identified cox1 intronic polymorphisms and repetitive sequence dynamics can be used as key molecular regulation sites to regulate the energy metabolism of mycelium and fruiting body development, thereby improving its cultivation efficiency. In terms of germplasm preservation, the five genetic clusters identified in this study can be used as core germplasm resources, and the conserved mitochondrial genomic regions can be used as molecular markers for germplasm authenticity identification.

In conclusion, this study, through mitochondrial pan-genome analysis, systematically revealed the evolutionary characteristics and functional adaptability of the *H. marmoreus* mitochondrial genome, providing a theoretical basis for variety breeding, molecular marker development, and genetic resource conservation. Future research could focus on the following directions: (1) Investigating the mechanism of nucleo-mitochondrial interaction, combined with transcriptome or functional experiments, to explore the regulatory role of mitochondrial variations on phenotypes such as fruiting body development, and to develop specific molecular markers based on core variation sites for precision molecular breeding of *H. marmoreus*; (2) Expanding the application of the graphical pan-genome method to other edible and medicinal fungi, and enabling analyses of evolutionary networks and breeding history; (3) Designing mitochondrial-nuclear and cytoplasmic exchange experiments, inspired by Cytoplasmic Hybrid studies in plants, to evaluate the direct impact of mitochondrial variations on phenotypes and environmental adaptability.

5. Conclusions

This study constructed the first graph-based mitochondrial pan-genome of *H. marmoreus* by integrating 31 mitochondrial genomes, systematically revealing the structural diversity and adaptive evolution mechanism of its mitochondrial genome. The identified 8 gene rearrangement patterns, 5

© 2025 by the author(s). Distributed under a Creative Commons CC BY license.

Preprints.org (www.preprints.org) | NOT PEER-REVIEWED | Posted: 28 February 2026 doi:10.20944/preprints202602.1502.v1

genetic clusters and abundant genetic variations provide breeding-relevant genetic markers and genomic framework for the germplasm resource improvement, molecular breeding and molecular regulation of *H. marmoreus*. For the cultivation of edible fungi, the results of this study provide a new molecular regulation strategy for improving the cultivation efficiency of *H. marmoreus*; in terms of germplasm preservation, it provides a scientific basis for the classification, identification and core germplasm selection of *H. marmoreus* germplasm resources. In addition, the graph-based mitochondrial pan-genome construction method used in this study can be extended to other edible and medicinal fungi, providing a new technical approach for the pan-genome research and molecular breeding of edible fungi.

Author Contributions: Conceptualization, R.M. and W.L.; Methodology, Y.W., R.M. and W.L.; Software, R.M., W.L. and Y.M.; Formal analysis, R.Y., Y.S., J.S., Y.L. and Y.G.; Investigation, R.M. and W.L.; Data curation, R.M. and W.L.; Writing - original draft preparation, R.M. and W.L.; Writing-review and editing, Y.M., D.B. and Y.W.; Visualization, R.M. and W.L.; Supervision, Y.M., D.B. and Y.W.; Project administration, Y.W.; Funding acquisition, D.B. and Y.W. All authors have read and agreed to the published version of the manuscript.

Funding: This research was funded by the National Natural Science Foundation of China (32372789) and the Excellent Team Plan of Shanghai Academy of Agricultural Sciences (2022)014.

Institutional Review Board Statement: Not applicable.

Informed Consent Statement: Not applicable.

Data Availability Statement: The public genomic information of strains f2, f4, nn12-1 and nn12-17 can be found respectively in the Genbank database (PV946885, PX600725, PX600726, PX600727). At the same time, this article related code uploaded to making the database (GitHub - maruichenzhanghao/Hypsizygus-marmoreus-mito-Pan-genome: A graph-based pan-genome constructed from the mitochondrial genomes of 31 *Hypsizygus marmoreus* strains.).

Acknowledgments: We extend our sincere gratitude to Professor Jianzhong Wu (Zhejiang Shouxiangu Botanical Drug Institute Co., Ltd., Hangzhou, China) and Professor Shijun Xiao (Jilin Agricultural University, China) for their expert guidance on genome sequencing methodologies and bioinformatics analysis.

Conflicts of Interest: The authors declare that they have no conflict of interest.

References

1. Wu, Y.; Peng, Q.; Kang, Q.; Zhou, C.; Li, Y.; Li, J.; Chen, H.; Bao, D. Comparative profiling of volatile compounds in white and brown *Hypsizygus marmoreus* during fruiting body development and postharvest storage. *J. Food Compos. Anal.* **2024**, *136*, 106800. doi:10.1016/j.jfca.2024.106800.
2. Min, B.; Kim, S.; Oh, Y.L.; Kong, W.S.; Park, H.; Cho, H.; Jang, K.Y.; Kim, J.G.; Choi, I.G. Genomic discovery of the hypsin gene and biosynthetic pathways for terpenoids in *Hypsizygus marmoreus*. *BMC Genomics* **2018**, *19*, 789. doi:10.1186/s12864-018-5159-y.
3. Wang, G.; Chen, L.; Tang, W.; Wang, Y.; Zhang, Q.; Wang, H.; Zhou, X.; Wu, H.; Guo, L.; Dou, M.; et al. Identifying a melanogenesis-related candidate gene by a high-quality genome assembly and population diversity analysis in *Hypsizygus marmoreus*. *J Genet Genomics* **2021**, *48*, 75-87. doi:10.1016/j.jgg.2021.01.002.
4. Wang, G.; Wang, Y.; Chen, L.; Wang, H.; Guo, L.; Zhou, X.; Dou, M.; Wang, B.; Lin, J.; Liu, L.; *et al*. Genetic structure and evolutionary diversity of mating-type (MAT) loci in *Hypsizygus marmoreus*. *IMA Fungus* **2021**, *12*, 35. doi:10.1186/s43008-021-00086-8.
5. Wu, Y.Y.; Shang, J.J.; Li, Y.; Zhou, C.L.; Hou, D.; Li, J.L.; Tan, Q.; Bao, D.P.; Yang, R.H. The complete mitochondrial genome of the Basidiomycete edible fungus *Hypsizygus marmoreus*. *Mitochondrial DNA B Resour* **2018**, *3*, 1241-1243. doi:10.1080/23802359.2018.1532343.
6. Wang, G.; Lin, J.; Shi, Y.; Chang, X.; Wang, Y.; Guo, L.; Wang, W.; Dou, M.; Deng, Y.; Ming, R.; et al. Mitochondrial genome in *Hypsizygus marmoreus* and its evolution in Dikarya. *BMC Genomics* **2019**, *20*, 765. doi:10.1186/s12864-019-6133-z.

© 2025 by the author(s). Distributed under a Creative Commons CC BY license.

Preprints.org (www.preprints.org) | NOT PEER-REVIEWED | Posted: 28 February 2026 doi:10.20944/preprints202602.1502.v1

7. Sandor, S.; Zhang, Y.; Xu, J. Fungal mitochondrial genomes and genetic polymorphisms. *Appl. Microbiol. Biotechnol.* **2018**, *102*, 9433-9448. doi:10.1007/s00253-018-9350-5.
8. Aguileta, G.; de Vienne, D.M.; Ross, O.N.; Hood, M.E.; Giraud, T.; Petit, E.; Gabaldón, T. High variability of mitochondrial gene order among fungi. *Genome Biol Evol* **2014**, *6*, 451-465. doi:10.1093/gbe/evu028.
9. Kim, S.; Song, Y.; Ha, B.; Moon, Y.J.; Kim, M.; Ryu, H.; Ro, H.S. Variable Number Tandem Repeats in the Mitochondrial DNA of *Lentinula edodes*. *Genes (Basel)* **2019**, *10*, 542. doi:10.3390/genes10070542.
10. Song, X.; Zhang, M.; Chen, M.; Shang, X.; Zhou, F.; Yu, H.; Song, C.; Tan, Q. Transcriptomic Communication between Nucleus and Mitochondria during the Browning Process of *Lentinula edodes*. *J. Agric. Food. Chem.* **2024**, *72*, 23592-23605. doi:10.1021/acs.jafc.4c03506.
11. Wu, P.; Bao, Z.; Tu, W.; Li, L.; Xiong, C.; Jin, X.; Li, P.; Gui, M.; Huang, W.; Li, Q. The mitogenomes of two saprophytic Boletales species (*Coniophora*) reveals intron dynamics and accumulation of plasmid-derived and non-conserved genes. *Computational and Structural Biotechnology Journal* **2021**, *19*, 401-414. doi:10.1016/j.csbj.2020.12.041.
12. Tan, H.; Yu, Y.; Fu, Y.; Liu, T.; Wang, Y.; Peng, W.; Wang, B.; Chen, J. Comparative analyses of *Flammulina filiformis* mitochondrial genomes reveal high length polymorphism in intergenic regions and multiple intron gain/loss in cox1. *Int. J. Biol. Macromol.* **2022**, *221*, 1593-1605. doi:10.1016/j.ijbiomac.2022.09.110.
13. Zhang, M.-Z.; Xu, J.-P.; Callac, P.; Chen, M.-Y.; Wu, Q.; Wach, M.; Mata, G.; Zhao, R.-L. Insight into the evolutionary and domesticated history of the most widely cultivated mushroom *Agaricus bisporus* via mitogenome sequences of 361 global strains. *BMC Genomics* **2023**, *24*, 182. doi:10.1186/s12864-023-09257-w.
14. Brankovics, B.; Kulik, T.; Sawicki, J.; Bilska, K.; Zhang, H.; de Hoog, G.S.; van der Lee, T.A.; Waalwijk, C.; van Diepeningen, A.D. First steps towards mitochondrial pan-genomics: detailed analysis of *Fusarium graminearum* mitogenomes. *PeerJ* **2018**, *6*, e5963. doi:10.7717/peerj.5963.
15. Wang, N.; Li, C.; Kuang, L.; Wu, X.; Xie, K.; Zhu, A.; Xu, Q.; Larkin, R.M.; Zhou, Y.; Deng, X.; et al. Pan-mitogenomics reveals the genetic basis of cytonuclear conflicts in citrus hybridization, domestication, and diversification. *Proc Natl Acad Sci U S A* **2022**, *119*, e2206076119. doi:10.1073/pnas.2206076119.
16. van Westerhoven, A.C.; Dijkstra, J.; Aznar Palop, J.L.; Wissink, K.; Bell, J.; Kema, G.H.J.; Seidl, M.F. Frequent genetic exchanges revealed by a pan-mitogenome graph of a fungal plant pathogen. *mBio* **2024**, e0275824. doi:10.1128/mbio.02758-24.
17. Kolmogorov, M.; Yuan, J.; Lin, Y.; Pevzner, P.A. Assembly of long, error-prone reads using repeat graphs. *Nat. Biotechnol.* **2019**, *37*, 540-546. doi:10.1038/s41587-019-0072-8.
18. Wick, R.R.; Schultz, M.B.; Zobel, J.; Holt, K.E. Bandage: interactive visualization of de novo genome assemblies. *Bioinformatics* **2015**, *31*, 3350-3352. doi:10.1093/bioinformatics/btv383.
19. Jin, J.J.; Yu, W.B.; Yang, J.B.; Song, Y.; dePamphilis, C.W.; Yi, T.S.; Li, D.Z. GetOrganelle: a fast and versatile toolkit for accurate de novo assembly of organelle genomes. *Genome Biol* **2020**, *21*, 241. doi:10.1186/s13059-020-02154-5.
20. Lang, B.F.; Beck, N.; Prince, S.; Sarrasin, M.; Rioux, P.; Burger, G. Mitochondrial genome annotation with MFannot: a critical analysis of gene identification and gene model prediction. *Front Plant Sci* **2023**, *14*, 1222186. doi:10.3389/fpls.2023.1222186.
21. Bernt, M.; Donath, A.; Jühling, F.; Externbrink, F.; Florentz, C.; Fritzsch, G.; Pütz, J.; Middendorf, M.; Stadler, P.F. MITOS: improved de novo metazoan mitochondrial genome annotation. *Mol Phylogenet Evol* **2013**, *69*, 313-319. doi:10.1016/j.ympev.2012.08.023.
22. Lowe, T.M.; Eddy, S.R. tRNAscan-SE: A Program for Improved Detection of Transfer RNA Genes in Genomic Sequence. *Nucleic Acids Res.* **1997**, *25*, 955-964. doi:10.1093/nar/25.5.955.
23. Ponty, Y.; Leclerc, F. Drawing and Editing the Secondary Structure(s) of RNA. In *RNA Bioinformatics*, Picardi, E., Ed.; Springer New York: New York, NY, 2015; pp. 63-100.
24. Beier, S.; Thiel, T.; Münch, T.; Scholz, U.; Mascher, M. MISA-web: a web server for microsatellite prediction. *Bioinformatics* **2017**, *33*, 2583-2585. doi:10.1093/bioinformatics/btx198.
25. Xiang, C.-Y.; Gao, F.; Jakovlić, I.; Lei, H.-P.; Hu, Y.; Zhang, H.; Zou, H.; Wang, G.-T.; Zhang, D. Using PhyloSuite for molecular phylogeny and tree-based analyses. *iMeta* **2023**, *2*, e87. doi:10.1002/imt2.87.
26. Tamura, K.; Stecher, G.; Kumar, S. MEGA11: Molecular Evolutionary Genetics Analysis Version 11. *Mol Biol Evol* **2021**, *38*, 3022-3027. doi:10.1093/molbev/msab120.

© 2025 by the author(s). Distributed under a Creative Commons CC BY license.

Preprints.org (www.preprints.org) | NOT PEER-REVIEWED | Posted: 28 February 2026 doi:10.20944/preprints202602.1502.v1

27. Katoh, K.; Standley, D.M. MAFFT multiple sequence alignment software version 7: improvements in performance and usability. *Mol Biol Evol* **2013**, *30*, 772-780. doi:10.1093/molbev/mst010.
28. Xu, B.; Yang, Z. PAMLX: a graphical user interface for PAML. *Mol Biol Evol* **2013**, *30*, 2723-2724. doi:10.1093/molbev/mst179.
29. Rozas, J.; Ferrer-Mata, A.; Sánchez-DelBarrio, J.C.; Guirao-Rico, S.; Librado, P.; Ramos-Onsins, S.E.; Sánchez-Gracia, A. DnaSP 6: DNA Sequence Polymorphism Analysis of Large Data Sets. *Mol Biol Evol* **2017**, *34*, 3299-3302. doi:10.1093/molbev/msx248.
30. Page, A.J.; Taylor, B.; Delaney, A.J.; Soares, J.; Seemann, T.; Keane, J.A.; Harris, S.R. SNP-sites: rapid efficient extraction of SNPs from multi-FASTA alignments. *Microb Genom* **2016**, *2*, e000056, doi:10.1099/mgen.0.000056.
31. Alexander, D.H.; Novembre, J.; Lange, K. Fast model-based estimation of ancestry in unrelated individuals. *Genome Res* **2009**, *19*, 1655-1664. doi:10.1101/gr.094052.109.
32. Minh, B.Q.; Schmidt, H.A.; Chernomor, O.; Schrempf, D.; Woodhams, M.D.; von Haeseler, A.; Lanfear, R. IQ-TREE 2: New Models and Efficient Methods for Phylogenetic Inference in the Genomic Era. *Mol Biol Evol* **2020**, *37*, 1530-1534. doi:10.1093/molbev/msaa015.
33. Letunic, I.; Bork, P. Interactive Tree of Life (iTOL) v6: recent updates to the phylogenetic tree display and annotation tool. *Nucleic Acids Res.* **2024**, *52*, w78-w82. doi:10.1093/nar/gkae268.
34. Emms, D.M.; Kelly, S. OrthoFinder: phylogenetic orthology inference for comparative genomics. *Genome Biol* **2019**, *20*, 238. doi:10.1186/s13059-019-1832-y.
35. Hickey, G.; Monlong, J.; Ebler, J.; Novak, A.M.; Eizenga, J.M.; Gao, Y.; Abel, H.J.; Antonacci-Fulton, L.L.; Asri, M.; Baid, G.; et al. Pangenome graph construction from genome alignments with Minigraph-Cactus. *Nat. Biotechnol.* **2024**, *42*, 663-673. doi:10.1038/s41587-023-01793-w.
36. Hickey, G.; Heller, D.; Monlong, J.; Sibbesen, J.A.; Sirén, J.; Eizenga, J.; Dawson, E.T.; Garrison, E.; Novak, A.M.; Paten, B. Genotyping structural variants in pangenome graphs using the vg toolkit. *Genome Biology* **2020**, *21*, 35. doi:10.1186/s13059-020-1941-7.
37. Li, H. A statistical framework for SNP calling, mutation discovery, association mapping and population genetical parameter estimation from sequencing data. *Bioinformatics* **2011**, *27*, 2987-2993. doi:10.1093/bioinformatics/btr509.
38. Guarracino, A.; Heumos, S.; Nahnsen, S.; Prins, P.; Garrison, E. ODGI: understanding pangenome graphs. *Bioinformatics* **2022**, *38*, 3319-3326. doi:10.1093/bioinformatics/btac308.
39. Zeb, U.; Aziz, T.; Azizullah, A.; Zan, X.Y.; Khan, A.A.; Bacha, S.A.S.; Cui, F.J. Complete mitochondrial genomes of edible mushrooms: features, evolution, and phylogeny. *Physiol. Plant.* **2024**, *176*, e14363. doi:10.1111/ppl.14363.
40. Tang, J.; Zhang, L.; Su, J.; Ye, Q.; Li, Y.; Liu, D.; Cui, H.; Zhang, Y.; Ye, Z. Insights into Fungal Mitochondrial Genomes and Inheritance Based on Current Findings from Yeast-like Fungi. *J Fungi (Basel)* **2024**, *10*, 441. doi:10.3390/jof10070441.
41. Kim, S.; Eom, H.; Nandre, R.; Choi, Y.J.; Lee, H.; Ryu, H.; Ro, H. S. Comparative structural analysis on the mitochondrial DNAs from various strains of *Lentinula edodes*. *Frontiers in Microbiology* **2022**, 13, 1034387. doi:10.3389/fmicb.2022.1034387.
42. Gao, W.; Chen, X.; He, J.; Sha, A.; Luo, Y.; Xiao, W.; Xiong, Z.; Li, Q. Intraspecific and interspecific variations in the synonymous codon usage in mitochondrial genomes of 8 *pleurotus* strains. *BMC Genomics* **2024**, *25*, 456. doi:10.1186/s12864-024-10374-3.
43. Li, Q.; Xiang, D.; Wan, Y.; Wu, Q.; Wu, X.; Ma, C.; Song, Y.; Zhao, G.; Huang, W. The complete mitochondrial genomes of five important medicinal *Ganoderma* species: Features, evolution, and phylogeny. *Int. J. Biol. Macromol.* **2019**, *139*, 397-408. doi:10.1016/j.ijbiomac.2019.08.003.
44. Liu, C.; Li, W.Y.; Zheng, L.X.; Dao, M.; Chen, H.H.; Han, L.H. Comparative mitogenomic analysis reveals variations and evolution of ectomycorrhizal fungal *Strobilomyces*. *IMA Fungus* **2025**, *16*, e141848. doi:10.3897/imafungus.16.141848.
45. Kang, M.; Wu, H.; Liu, H.; Liu, W.; Zhu, M.; Han, Y.; Liu, W.; Chen, C.; Song, Y.; Tan, L.; et al. The pan-genome and local adaptation of *Arabidopsis thaliana*. *Nat. Commun.* **2023**, *14*, 6259. doi:10.1038/s41467-023-42029-4.

© 2025 by the author(s). Distributed under a Creative Commons CC BY license.

Preprints.org (www.preprints.org) | NOT PEER-REVIEWED | Posted: 28 February 2026 doi:10.20944/preprints202602.1502.v1

46. Waneka, G.; Svendsen, J.M.; Havird, J.C.; Sloan, D.B. Mitochondrial mutations in *Caenorhabditis elegans* show signatures of oxidative damage and an AT-bias. *Genetics* **2021**, *219*, iyab116. doi:10.1093/genetics/iyab116.
47. Boore, J.L. Animal mitochondrial genomes. *Nucleic Acids Res.* **1999**, *27*, 1767-1780. doi:10.1093/nar/27.8.1767.
48. Gualberto, J.M.; Newton, K.J. Plant Mitochondrial Genomes: Dynamics and Mechanisms of Mutation. *Annu Rev Plant Biol* **2017**, *68*, 225-252. doi:10.1146/annurev-arplant-043015-112232.
49. Tao, G.; Ahrendt, S.; Miyauchi, S.; Zhu, X.; Peng, H.; Labutti, K.; Clum, A.; Hayes, R.; Chain, P.S.G.; Grigoriev, I.V.; et al. Characterisation and comparative analysis of mitochondrial genomes of false, yellow, black and blushing morels provide insights on their structure and evolution. *IMA Fungus* **2025**, *16*, e138363. doi:10.3897/imafungus.16.138363.
50. Al-Reedy, R.M.; Malireddy, R.; Dillman, C.B.; Kennell, J.C. Comparative analysis of Fusarium mitochondrial genomes reveals a highly variable region that encodes an exceptionally large open reading frame. *Fungal genetics and biology : FG & B* **2012**, *49*, 2-14. doi:10.1016/j.fgb.2011.11.008.
51. Basse, C.W. Mitochondrial inheritance in fungi. *Current opinion in microbiology* **2010**, *13*, 712-719. doi:10.1016/j.mib.2010.09.003.
52. Deng, Y.; Hsiang, T.; Li, S.; Lin, L.; Wang, Q.; Chen, Q.; Xie, B.; Ming, R. Comparison of the Mitochondrial Genome Sequences of Six *Annulohypoxylon stygium* Isolates Suggests Short Fragment Insertions as a Potential Factor Leading to Larger Genomic Size. *Front Microbiol* **2018**, *9*, 2079. doi:10.3389/fmicb.2018.02079.
53. Kolesnikova, A.I.; Putintseva, Y.A.; Simonov, E.P.; Biriukov, V.V.; Oreshkova, N.V.; Pavlov, I.N.; Sharov, V.V.; Kuzmin, D.A.; Anderson, J.B.; Krutovsky, K.V. Mobile genetic elements explain size variation in the mitochondrial genomes of four closely-related *Armillaria* species. *BMC Genomics* **2019**, *20*, 351. doi:10.1186/s12864-019-5732-z.
54. Barroso, G.; Bois, F.; Labarère, J. Duplication of a truncated paralog of the family B DNA polymerase gene *Aa-polB* in the *Agrocybe aegerita* mitochondrial genome. *Appl. Environ. Microbiol.* **2001**, *67*, 1739-1743. doi:10.1128/aem.67.4.1739-1743.2001.
55. Adams, K.L.; Palmer, J.D. Evolution of mitochondrial gene content: gene loss and transfer to the nucleus. *Molecular phylogenetics and evolution* **2003**, *29*, 380-395. doi:10.1016/s1055-7903(03)00194-5.
56. Wang, X.; Wei, S.; Wu, S.; Tang, J.; Wei, J.; Liu, Z.; Qi, L. Characterization and phylogenetic analysis of the complete mitochondrial genome sequence of Auricularia villosula, an edible wild mushroom in China. *Biologia* **2023**, *78*, 3713-3723. doi:10.1007/s11756-023-01533-0.
57. Li, Q.; Zhang, T.; Li, L.; Bao, Z.; Tu, W.; Xiang, P.; Wu, Q.; Li, P.; Cao, M.; Huang, W. Comparative Mitogenomic Analysis Reveals Intraspecific, Interspecific Variations and Genetic Diversity of Medical Fungus *Ganoderma*. *Journal of Fungi* **2022**, *8*, 781.
58. Wang, X.; Wang, G.; Tao, J.; Guo, Z.; Xu, G.; Li, J.; Kang, J.; Zuo, Q.; Liu, H.; Li, Q. Comparative analysis of mitochondrial genomes in lycoperdaceae fungi reveals intron dynamics and phylogenetic relationships. *BMC Genomics* **2025**, *26*, 742. doi:10.1186/s12864-025-11911-4.
59. Goddard, M.R.; Burt, A. Recurrent invasion and extinction of a selfish gene. *Proceedings of the National Academy of Sciences* **1999**, *96*, 13880-13885. doi:10.1073/pnas.96.24.13880.
60. Mukhopadhyay, J.; Wai, A.; Lang, B.F.; Hausner, G. Characterization of the mitochondrial genomes for *Ophiostomaips* and related taxa from various geographic origins and related species: large intron-rich genomes and complex intron arrangements. *IMA Fungus* **2025**, *16*, e159349. doi:10.3897/imafungus.16.159349.

Disclaimer/Publisher's Note: The statements, opinions and data contained in all publications are solely those of the individual author(s) and contributor(s) and not of MDPI and/or the editor(s). MDPI and/or the editor(s) disclaim responsibility for any injury to people or property resulting from any ideas, methods, instructions or products referred to in the content.

© 2025 by the author(s). Distributed under a Creative Commons CC BY license.